



Please cite the Published Version

Hussein, M. S. , Dyhoum, Taysir E, Hussein, S. O.  and Qassim, Mohammed (2024) Identification of time-wise thermal diffusivity, advection velocity on the free-boundary inverse coefficient problem. *Mathematics*, 12 (17). 2629 ISSN 2227-7390

DOI: <https://doi.org/10.3390/math12172629>

Publisher: MDPI

Version: Published Version

Downloaded from: <https://e-space.mmu.ac.uk/635449/>

Usage rights:  [Creative Commons: Attribution 4.0](https://creativecommons.org/licenses/by/4.0/)

Additional Information: This is an open access article which first appeared in *Mathematics*, published by MDPI



Data Access Statement: The original contributions presented in the study are included in the article, further inquiries can be directed to the corresponding authors.

Enquiries:

If you have questions about this document, contact openresearch@mmu.ac.uk. Please include the URL of the record in e-space. If you believe that your, or a third party's rights have been compromised through this document please see our Take Down policy (available from <https://www.mmu.ac.uk/library/using-the-library/policies-and-guidelines>)

Article

Identification of Time-Wise Thermal Diffusivity, Advection Velocity on the Free-Boundary Inverse Coefficient Problem

M. S. Hussein ¹, Taysir E. Dyhoum ^{2,3,*}, S. O. Hussein ^{4,*} and Mohammed Qassim ⁵

¹ Department of Mathematics, College of Science, University of Baghdad, Baghdad 10071, Iraq; mmmsh@sc.uobaghdad.edu.iq

² Department of Computing and Mathematics, Faculty of Science and Engineering, Manchester Metropolitan University, Manchester M15 6BX, UK

³ Department of Mathematics, Misurata University, Misurata P.O. Box 2478, Libya

⁴ Department of Mathematics, College of Science, University of Sulaymaniyah, Sulaymaniyah 46001, Iraq

⁵ Department of Energy, College of Engineering Al-Musayab, University of Babylon, Babylon 51002, Iraq; mq63582@gmail.com

* Correspondence: t.dyhoum@mmu.ac.uk (T.E.D.); shilan.husen@univsul.edu.iq (S.O.H.)

Abstract: This paper is concerned with finding solutions to free-boundary inverse coefficient problems. Mathematically, we handle a one-dimensional non-homogeneous heat equation subject to initial and boundary conditions as well as non-localized integral observations of zeroth and first-order heat momentum. The direct problem is solved for the temperature distribution and the non-localized integral measurements using the Crank–Nicolson finite difference method. The inverse problem is solved by simultaneously finding the temperature distribution, the time-dependent free-boundary function indicating the location of the moving interface, and the time-wise thermal diffusivity or advection velocities. We reformulate the inverse problem as a non-linear optimization problem and use the *lsqnonlin* non-linear least-square solver from the MATLAB optimization toolbox. Through examples and discussions, we determine the optimal values of the regulation parameters to ensure accurate, convergent, and stable reconstructions. The direct problem is well-posed, and the Crank–Nicolson method provides accurate solutions with relative errors below 0.006% when the discretization elements are $M = N = 80$. The accuracy of the forward solutions helps to obtain sensible solutions for the inverse problem. Although the inverse problem is ill-posed, we determine the optimal regularization parameter values to obtain satisfactory solutions. We also investigate the existence of inverse solutions to the considered problems and verify their uniqueness based on established definitions and theorems.

Keywords: parabolic heat equation; finite-difference method (FDM); Crank–Nicolson method; inverse coefficient identification problem; optimization tool; MATLAB; free-boundary problem

MSC: 65K05; 65K10; 65R30; 65R32; 65Y15; 65Y15; 65N12



Citation: Hussein, M.S.; Dyhoum, T.E.; Hussein, S.O.; Qassim, M. Identification of Time-Wise Thermal Diffusivity, Advection Velocity on the Free-Boundary Inverse Coefficient Problem. *Mathematics* **2024**, *12*, 2629. <https://doi.org/10.3390/math12172629>

Academic Editors: Tao Liu, Fazlollah Soleymani, Qiang Ma and Cheng-Hung Huang

Received: 17 May 2024

Revised: 6 August 2024

Accepted: 9 August 2024

Published: 24 August 2024



Copyright: © 2024 by the authors. Licensee MDPI, Basel, Switzerland. This article is an open access article distributed under the terms and conditions of the Creative Commons Attribution (CC BY) license (<https://creativecommons.org/licenses/by/4.0/>).

1. Introduction

Partial differential equations (PDEs) subject to various non-local initial and boundary conditions are common expressions of mathematical models that arise when solving real-world problems. These real-world applications emerge in several scientific and engineering disciplines and fields, including geology, hydrodynamics, biological fluid dynamics, vibration materials, heat transfer, control theory, and thermoelastic problems [1–7]. Recent work on flow, heat, and thermal conductivity considers essential physical aspects, including Thompson and Troian slip effects on ternary hybrid nanofluid flow across a porous plate with a chemical reaction [8].

Due to the difficulty of obtaining analytical solutions, researchers employ various mathematical, statistical, and computer vision techniques to generate numerical approximated values to determine PDE systems' direct and inverse solutions. The sought solutions

are represented by various physical quantities and medium properties, such as potential and damping parameters [9], the force source function [4], constant voltage and values of contact impedance [10], and reaction coefficients [5]. Such quantities appear as unknown time- and space-dependent coefficients or functions in the model, turning the problem into inverse coefficient problems (ICPs). Many empirical and theoretical studies focused on adapting and applying numerical techniques to solve ICPs. These include implicit finite difference methods [11,12], lattice-free finite difference methods [13], Fourier regularization to solve one-dimensional non-local coefficient heat problems [14], the collocation method [15], and iterative boundary element methods [16,17].

In this work, we consider solving ICPs with free-boundary (non-local) conditions. These conditions can mathematically represent phase-changing processes such as the freezing of water or the ground, solidifying of metals, melting of ice, forming of crystals, evaporation of chemicals, and so on, in which the heat associated with the phase change is either generated or absorbed [18–20]. Finding the solutions means determining the domain's temperature distribution, the location of the movable boundaries and dynamic interface, and the unknown functions of time-wise thermal diffusivity or time- and space-dependent diffusion. This process poses a significant computational challenge, requiring numerical strategies to accurately estimate free boundaries and complex energetic interfacing. Because these inverse problems are ill-posed, we ensure that the solutions exist and are unique (locally) by aligning the considered cases with previous theoretical studies [21–23]. To investigate the inverse problem with non-localized conditions, we structure the model as a non-homogeneous one-dimensional heat equation subject to a set of initial and boundary conditions plus over-determined conditions of the zeroth and first-order heat momentum.

In this study, we apply the Crank–Nicolson (CN) finite difference method to solve the free-boundary (non-local) problem. We then utilize Tikhonov regularization techniques to stabilize the inverse problem and sort out the non-linearity issue by using the MATLAB R2023a optimization toolbox *lsqnonlin*. We find the time-dependent free-boundary function, which indicates the location of the moving interface, the temperature distribution at the boundaries, and the time-wise thermal diffusivity or advection velocities simultaneously. There are many alternative techniques to solve similar problems. For example, Martín-Vaquero and Sajavičius [24] used the two-level finite difference method (FDM) to solve one-dimensional parabolic equations subject to initial conditions represented in non-local discrete integrals and other homogeneous boundary conditions. A minimal surface equation, a two-dimensional nonlinear elliptic equation subject to additional boundary non-local integral conditions, has been solved iteratively using a system of difference equation approximations [2]. A novel iteration scheme based on the domain decomposition method is applied to determine the time-dependent coefficients in heat and Volterra integral equations, as presented in [7,25]. Recently, Huntul and Lesnic [26,27] used multilevel finite difference approximations to retrieve unknown time-dependent intensity and convection coefficients in free-boundary two-dimensional heat problems. We have previously used this numerical approach to identify the temperature distribution and other time-dependent parameters, such as the intensity of reaction, perfusion, and radioactive coefficients, based on over-specified conditions of Stefan-type, zeroth-order heat momentum [28,29].

This paper is organized as follows. In Section 2, the mathematical formulations of the problem are set up, including ensuring that the existence and uniqueness requirements are satisfied. The use of the CN technique to identify the problem's forward solutions is demonstrated in Section 3. We calculate the inverse solutions in Section 4; this section covers the CN solver, Tikhonov's regularization method, and the *lsqnonlin* MATLAB solver. A couple of numerical examples (simulations) are discussed and investigated in Section 5. Section 6 summarizes the findings and suggests further research.

2. Mathematical Formulation

Consider the domain $D_T = \{(x, \tau) : 0 < x < s(\tau), 0 < \tau < T\}$ for the following mathematical problem. The primary goal of this research is to find the free boundary

$s(\tau)$, and the time-wise thermal diffusivity $a(\tau)$ or advection velocity $b(x, \tau)$. Thermal diffusivity is the heat transfer property of a medium; the advection velocity refers to the flow of molecules in the examined medium.

$$\frac{\partial}{\partial \tau} u(x, \tau) = a(\tau) \frac{\partial^2}{\partial x^2} u(x, \tau) + b(x, \tau) \frac{\partial}{\partial x} u(x, \tau) + c(x, \tau)u(x, \tau) + f(x, \tau), \quad \text{in } D_T, \quad (1)$$

is subject to the initial and non-homogeneous Dirichlet boundary conditions

$$u(x, 0) = \varphi(x), \quad 0 \leq x \leq s(\tau), \quad (2)$$

$$u(0, \tau) = \gamma_1(\tau), \quad u(s(\tau), \tau) = \gamma_2(\tau), \quad 0 \leq \tau \leq T, \quad (3)$$

where $\{c(x, \tau), f(x, \tau), \varphi(x), \gamma_1(\tau), \gamma_2(\tau)\}$ are given functions and $\{u(x, \tau), s(\tau), a(\tau), b(x, \tau)\}$ are unknown functions that will be numerically approximated.

If the functions $\{s(\tau), a(\tau), b(x, \tau)\}$ are given, Equations (1)–(3) form a direct well-posed problem. If some or all of the function terms $(s(\tau), a(\tau))$ or $(s(\tau), b(x, \tau))$ of Equations (1)–(3) are not defined, the above set of equations is insufficient to determine them uniquely. Such a situation leads to handling a solution of the inverse ill-posed problem [21]. In this case, we must impose additional data to retain uniqueness:

$$\int_0^{s(\tau)} x^\ell u(x, \tau) dx = \gamma_{3+\ell}(\tau), \quad \tau \in [0, T], \quad \ell \in \{0, 1\}. \quad (4)$$

Equation (4) represents the zeroth ($\ell = 0$) and first-order ($\ell = 1$) heat momentum. To solve the inverse ill-posed problem in Equations (1)–(4), we first convert the free domain function $s(\tau)$ to a fixed domain by setting $\eta = \frac{x}{s(\tau)}$ and $\tau = \tau$. This implies that $u(x, \tau) = u(\eta s(\tau), \tau) = v(\eta, \tau)$ and $Q_T = \{(\eta, \tau) : 0 < \eta < 1, \quad 0 < \tau < T\}$. Therefore, using the previous transformation, Equations (1)–(4) can be rewritten in compact notation as

$$v_\tau = \frac{a(\tau)}{s^2(\tau)} v_{\eta\eta} + \frac{b(\eta s(\tau), \tau) + \eta s'(\tau)}{s(\tau)} v_\eta + c(\eta s(\tau), \tau)v + f(\eta s(\tau), \tau), \quad (\eta, \tau) \in Q_T, \quad (5)$$

$$v(\eta, 0) = \varphi(s(0)\eta), \quad \eta \in [0, 1], \quad (6)$$

$$v(0, \tau) = \gamma_1(\tau), \quad v(1, \tau) = \gamma_2(\tau), \quad \tau \in [0, T], \quad (7)$$

$$s^{\ell+1}(\tau) \int_0^1 v(\eta, \tau) d\eta = \gamma_{3+\ell}(\tau), \quad \tau \in [0, T], \quad \ell \in \{0, 1\}. \quad (8)$$

Based on well-established theories on the uniqueness of this inverse problem [21–23], we assume the problem in Equations (5)–(8) requires the existence and uniqueness criteria as follows.

Definition 1. The solution of the inverse problem in Equations (5)–(8) can be:

Case 1. When $b(\eta s(\tau), \tau)$ is known, it is the triplet class $(a(\tau), s(\tau), v(\eta, \tau)) \in C[0, T] \times C^1[0, T] \times C^{2,1}(\overline{Q}_T)$.

Case 2. If $a(\tau)$ is given and $b(\eta s(\tau), \tau)$ only depends on time ($b(\eta s(\tau), \tau) = b(\tau)$), it is the triplet class $(s(\tau), b(\tau), v(\eta, \tau)) \in C^1[0, T] \times C[0, T] \times C^{2,1}(\overline{Q}_T)$, where $a(\tau) > 0$ and $s(\tau) > 0$ for $\tau \in [0, T]$.

Theorem 1. Consider the case where $b(\eta s(\tau), \tau)$ is known (Case 1) and assume the input data for the problem in Equations (5)–(8) satisfy the following three conditions:

1. $\gamma_i \in C^1[0, T], \gamma_i(\tau) > 0$, for $i = \overline{1, 4}, \gamma_4'(\tau) > 0, s(\tau)u_x(0, \tau) - \gamma_2(\tau) + \gamma_1(\tau) > 0, b(0, \tau)\gamma_1(\tau) + \gamma_3'(\tau) \leq 0$, for $\tau \in [0, T]$.
2. $\varphi \in C^2[0, s(0)], \varphi(x) > 0, \varphi'(x) > 0$, for $x \in [0, s(0)]$, where $s_0 = s(0) > 0$ by the solution of $\int_0^{s_0} h(0)\varphi(\eta s(0))d\eta = \gamma_3(0)$.

3. $b, c, f \in C^{1,0}([0, H_1] \times [0, T]), f(x, \tau) \geq 0, b(x, \tau) \geq 0, c(x, \tau) - b_x(x, \tau) \geq 0,$ for $(x, \tau) \in [0, H_1] \times [0, T]$ where, $H_1 = \max_{\tau \in [0, T]} \gamma_3(\tau) \left(\min_{x \in [0, s_0]} (\min_{\tau \in [0, T]} \varphi(x), \min_{\tau \in [0, T]} \gamma_1(\tau), \min_{\tau \in [0, T]} \gamma_2(\tau)) \right)^{-1}$.
4. $\varphi(0) = \gamma_1(0), \varphi(s(0)) = \gamma_2(0)$ and $s^2(0) \int_0^1 \eta \varphi(s(0)) d\eta = \gamma_4(0)$.

Then, there exists a unique solution for the inverse problem in Equations (5)–(8) where $\tau_0 \in [0, T]$ is defined as input data for this problem.

To solve the inverse problem in Equations (5)–(8) in **Case 1**, with given $b(\eta s(\tau), \tau)$, we start by finding the initial values of the unknown quantities $a(0)$ and $s'(0)$. This step is essential to find stable numerical reconstructions later. Then, we derive the derivative of the integral equations of the over-determination condition in Equation (4) concerning time:

$$\gamma'_{3+\ell}(\tau) = s^\ell(\tau) \gamma_2(\tau) s'(\tau) + \int_0^{s(\tau)} x^\ell u_\tau(x, \tau) dx. \quad \ell \in \{0, 1\}. \tag{9}$$

To obtain the second term on the right-hand side of Equation (9), we integrate the one-dimensional parabolic governing Equation (1) over the interval $[0, s(\tau)]$ with respect to space x . To get the second term on the right-hand side of Equation (9) when $\ell = 1$, we multiply Equation (1) by x and integrate over the same period

$$\int_0^{s(\tau)} u_\tau dx = a(\tau) [u_x(s(\tau), \tau) - u_x(0, \tau)] + \int_0^{s(\tau)} [b(x, \tau) u_x + c(x, \tau) u + f(x, \tau)] dx, \tag{10}$$

multiplying by x

$$\begin{aligned} \int_0^{s(\tau)} x u_\tau dx &= a(\tau) [s(\tau) u_x(s(\tau), \tau) - \gamma_2(\tau) + \gamma_1(\tau)] \\ &+ \int_0^{s(\tau)} x [b(x, \tau) u_x + c(x, \tau) u + f(x, \tau)] dx. \end{aligned} \tag{11}$$

Finally, by substituting Equation (10) into (9) ($\ell = 0$), Equation (11) into (9) ($\ell = 1$), and conducting some re-arrangements taking into account that $s'(\tau)$ and $a(\tau)$ are unknown functions, we obtain

$$\gamma_2(\tau) s'(\tau) + [u_x(s(\tau), \tau) - u_x(0, \tau)] a(\tau) = \gamma'_3(\tau) - \delta_1(\tau) := L_3(\tau),$$

$$s(\tau) \gamma_2(\tau) s'(\tau) + [s(\tau) u_x(s(\tau), \tau) - \gamma_2(\tau) + \gamma_1(\tau)] a(\tau) = \gamma'_4(\tau) - \delta_2(\tau) := L_4(\tau).$$

The above equations can be written in matrix form as

$$\begin{bmatrix} \gamma_2(\tau) & u_x(s(\tau), \tau) - u_x(0, \tau) \\ s(\tau) \gamma_2(\tau) & s(\tau) u_x(s(\tau), \tau) - \gamma_2(\tau) + \gamma_1(\tau) \end{bmatrix} \begin{bmatrix} s'(\tau) \\ a(\tau) \end{bmatrix} = \begin{bmatrix} L_3(\tau) \\ L_4(\tau) \end{bmatrix} \tag{12}$$

where

$$\delta_1(\tau) = \int_0^{s(\tau)} (b(x, \tau) u_x + c(x, \tau) u + f(x, \tau)) dx,$$

$$\delta_2(\tau) = \int_0^{s(\tau)} x (b(x, \tau) u_x + c(x, \tau) u + f(x, \tau)) dx.$$

To obtain a unique solution of the above 2×2 system, the determinant must not vanish in $[0, T]$,

$$\begin{aligned} \Delta_1(\tau) &= \left| \begin{array}{cc} \gamma_2(\tau) & u_x(s(\tau), \tau) - u_x(0, \tau) \\ s(\tau)\gamma_2(\tau) & s(\tau)u_x(s(\tau), \tau) - \gamma_2(\tau) + \gamma_1(\tau) \end{array} \right| \\ &= \gamma_2(\tau)[s(\tau)u_x(s(\tau), \tau) - \gamma_2 + \gamma_1] - s(\tau)\gamma_2[u_x(s(\tau), \tau) - u_x(0, \tau)] \\ &= s(\tau)\gamma_2(\tau)u_x(s(\tau), \tau) - \gamma_2^2(\tau) + \gamma_2(\tau)\gamma_1(\tau) - s(\tau)\gamma_2(\tau)u_x(s(\tau), \tau) + s(\tau)\gamma_2(\tau)u_x(0, \tau) \\ &= -\gamma_2^2(\tau) + \gamma_2(\tau)\gamma_1(\tau) + s(\tau)\gamma_2(\tau)\gamma_2(\tau)u_x(0, \tau). \end{aligned}$$

Therefore,

$$\begin{aligned} s'(\tau) &= \frac{L_4(\tau)u_x(0, \tau) + s(\tau)L_3(\tau)u_x(s(\tau), \tau) - L_4(\tau)u_x(s(\tau), \tau) + L_3(\tau)\gamma_1(\tau) - L_3(\tau)\gamma_2(\tau)}{\Delta_1(\tau)}, \\ a(\tau) &= \frac{\gamma_2(\tau)L_4(\tau) - \gamma_2(\tau)s(\tau)L_3(\tau)}{\Delta_1(\tau)}, \end{aligned}$$

and making $\tau = 0$ in the last two expressions results in

$$s'(0) = \frac{L_4(0)u_x(0, 0) + h(0)L_3(0)u_x(h_0, 0) - L_4(0)u_x(h_0, 0) + L_3(0)\gamma_1(0) - L_3(0)\gamma_2(0)}{\Delta_1(0)}, \tag{13}$$

$$a(0) = \frac{\gamma_2(0)L_4(0) - \gamma_2(0)h_0L_3(0)}{\Delta_1(0)}. \tag{14}$$

Theorem 2. Consider the case where $a(\tau) = 1$, the function $b(\eta s(\tau), \tau) = b(\tau)$ is unknown (**Case 2**), and the following conditions are satisfied:

1. $\gamma_i(\tau) \in C^1[0, 1]$, $\gamma_i(\tau) > 0$, $i = \overline{1, 4}$ and $f \in C([0, \infty) \times [0, T])$, $f(x, \tau) \geq 0$ for $x \in [0, +\infty)$, $\tau \in [0, T]$. Also, $\varphi \in C^2[0, s(0)]$, $\varphi'(x) > 0$ for $x \in [0, h(0)]$.
2. The compatibility conditions are

$$\begin{aligned} \varphi(0) &= \gamma_1(0), & \varphi(s(0)) &= \gamma_2(0), \\ \gamma_1'(0) &= \frac{1}{s^2(0)}\varphi''(0) + \frac{b(0)}{s(0)}\varphi'(0) + c(0, 0)\varphi(0) + f(0, 0), \\ \gamma_2'(0) &= \frac{1}{s^2(0)}\varphi''(s(0)) + \left[\frac{b(0)}{s(0)} + \frac{s'(0)}{h(0)} \right] \varphi'(h(0)) + c(s(0), 0)\varphi(s(0)) + f(s(0), 0). \end{aligned}$$

Then, we can determine $T_1 \in (0, T]$ such that there exists a local solution to the inverse problem in Equations (1)–(4) or (5)–(8) for $(y, \tau) \in Q_{T_1}$.

Theorem 3. Assume the following conditions hold for the previous case:

1. $f, c \in C^{1,0}([0, +\infty) \times [0, T])$,
2. $\varphi(x) \geq \varphi_0$ and $f(x, \tau) \geq 0$, for $x \in ([0, +\infty) \times [0, T])$,
3. $\gamma_i(\tau) > 0$, $i = \overline{1, 4}$ for $\tau \in [0, T]$ and $\varphi'(x) > 0$ for $x \in [0, h_0]$.

Then, the problem in Equations (5)–(8) cannot have more than one solution in the domain Q_{T_1} .

It is necessary to calculate the values of $s'(0)$ and $b(0)$ in **Case 2** to find the inverse solution of Equations (5)–(8). We apply the same approach used for **Case 1**. We find the equations corresponding to Equation (9) when $\ell \in \{0, 1\}$ and substitute $a(\tau) = 1$, $b(x, \tau) = b(\tau)$ into the equations corresponding to Equations (10) and (11), respectively. This yields

$$\int_0^{s(\tau)} u_\tau dx = \int_0^{s(\tau)} \left[u_{xx} + c(x, \tau)u + f(x, \tau) \right] dx + b(\tau) \int_0^{s(\tau)} u_x dx,$$

$$\int_0^{s(\tau)} xu_\tau dx = \int_0^{s(\tau)} x \left[u_{xx} + c(x, \tau)u + f(x, \tau) \right] dx + b(\tau) \int_0^{s(\tau)} xu_x dx.$$

Then, we apply integration by parts to calculate the exact values of the latest τ terms in the previous equations, which leads to the following equations. In addition, we replace them with Equation (9) ($\ell \in \{0, 1\}$):

$$\gamma_2(\tau)s'(\tau) + [\gamma_2(\tau) - \gamma_1(\tau)]b(\tau) = \gamma_3'(\tau) - \int_0^{s(\tau)} [u_{xx} + c(x, \tau)u + f(x, \tau)] dx = L_1(\tau),$$

$$s(\tau)\gamma_2(\tau)s'(\tau) + [s(\tau)\gamma_2(\tau) - \gamma_3(\tau)]b(\tau) = \gamma_4'(\tau) - \int_0^{s(\tau)} x[u_{xx} + c(x, \tau)u + f(x, \tau)] dx = L_2(\tau).$$

To join the previous differential equations, we express them in the following matrix form:

$$\begin{bmatrix} \gamma_2(\tau) & \gamma_2(\tau) - \gamma_1(\tau) \\ \gamma_2(\tau)s(\tau) & s(\tau)\gamma_2(\tau) - \gamma_3(\tau) \end{bmatrix} \begin{bmatrix} s'(\tau) \\ b(\tau) \end{bmatrix} = \begin{bmatrix} L_1(\tau) \\ L_2(\tau) \end{bmatrix},$$

where

$$s'(\tau) = \frac{(\gamma_1(\tau) - \gamma_2(\tau))L_2(\tau) + L_1(\tau)(s(\tau)\gamma_2(\tau) - \gamma_3(\tau))}{\gamma_2(s(\tau)\gamma_1(\tau) - \gamma_3(\tau))} \quad \tau \in [0, T],$$

$$b(\tau) = \frac{-s(\tau)L_1(\tau) + L_2(\tau)}{s(\tau)\gamma_1(\tau) - \gamma_3(\tau)} \quad \tau \in [0, T],$$

and setting $\tau = 0$ results in

$$s'(0) = \frac{(\gamma_1(0) - \gamma_2(0))L_2(0) + L_1(0)(s(0)\gamma_2(0) - \gamma_3(0))}{\gamma_2(0)(s(0)\gamma_1(0) - \gamma_3(0))}, \tag{15}$$

$$b(0) = \frac{-s(0)L_1(0) + L_2(0)}{s(0)\gamma_1(0) - \gamma_3(0)}. \tag{16}$$

Equations (15) and (16) are both required for compatibility with Condition 2 of Theorem 2 to prove the existence of the solutions to the problem in Equations (5)–(8).

3. Applied CN Method to Obtain the Direct Solutions to the Problem

In this section, we take into account the initial boundary value problem in Equations (5)–(7), where $\{a(\tau), b(\eta s(\tau), \tau), c(\eta s(\tau), \tau), \varphi(\eta s(0)), \gamma_i(\tau)\}$ with $i = 1, 2$ are known functions that meet the existence and uniqueness conditions in Theorems 1–3. We seek to compute the direct solution $v(\eta, \tau)$. Furthermore, we can figure out the numerical values of Equation (8) ($\ell \in \{0, 1\}$) by employing the CN finite difference method. This method is unconditionally stable, and the solutions have second-order accuracy in the time and spatial dimensions.

To discretize the domain $Q_T = (0, 1) \times (0, T)$, we divide it into small M and N intervals of equally spaced length $\Delta\eta$ and $\Delta\tau$, denoting the uniform space and time increments by $\Delta\eta = \frac{1}{M}$ and $\Delta\tau = \frac{T}{N}$, respectively. We refer to the solution at the node point (i, j) as $v_{i,j} = v(\eta_i, \tau_j)$, $a(\tau_j) = a_j$, $b(\eta_i, \tau_j) = b_{i,j}$, $c(\eta_i, \tau_j) = c_{i,j}$, and $f(\eta_i, \tau_j) = f_{i,j}$, where $\eta_i = i\Delta\eta$, $\tau_j = j\Delta\tau$ for $i = 0, M, j = 0, N$ [4,30].

We rename the right-hand side of Equation (5) as $\Theta(\tau, \eta, v, v_\eta, v_{\eta\eta})$, i.e.,

$$\Theta(\tau, \eta, v, v_\eta, v_{\eta\eta}) = \frac{a(\tau)}{s^2(\tau)}v_{\eta\eta} + \left(\frac{b(\eta s(\tau), \tau) + s'(\tau)\eta}{s(\tau)} \right)v_\eta + c(\eta s(\tau), \tau)v + f(\eta s(\tau), \tau), (\eta, \tau) \in Q_T.$$

By discretizing the previous equation using the FDM, we obtain

$$\Theta_{i,j} = \left(\frac{a(\tau_j)}{s^2(\tau_j)} \right) \frac{v_{i+1,j} - 2v_{i,j} + v_{i-1,j}}{\Delta\eta^2} + \left(\frac{b(\eta_i s(\tau_j)) + s'(\tau_j)y_i}{s(\tau_j)} \right) \frac{v_{i+1,j} - v_{i-1,j}}{2\Delta\eta} + c_{i,j}v_{i,j} + f_{i,j}, \quad i = \overline{0, M}, \quad j = \overline{0, N}.$$

Benefiting from the fact that CN techniques are unconditionally stable and provide convergence of the second order in time and space for such problems [12,31,32], we apply them to Equations (5)–(7) to obtain

$$\frac{v_{i,j+1} - v_{i,j}}{\Delta\tau} = \frac{1}{2}(\Theta_{i,j+1} + \Theta_{i,j}), \tag{17}$$

$$v(\eta_i, 0) = \varphi(\eta_i s(0)), \quad i = \overline{0, M}, \tag{18}$$

$$v(0, \tau_j) = \gamma_1(\tau_j), \quad v(1, \tau_j) = \gamma_2(\tau_j), \quad j = \overline{0, N}. \tag{19}$$

By substituting $\Theta_{i,j}$ and $\Theta_{i,j+1}$ into Equation (17), we obtain the system of equations

$$-A_{i,j+1}v_{i-1,j+1} + [1 - B_{i,j+1}]v_{i,j+1} - C_{i,j+1}v_{i+1,j+1} = A_{i,j}v_{i-1,j} + [1 + B_{i,j+1}]v_{i,j} + C_{i,j}v_{i+1,j} + \frac{\Delta\tau}{2}(f_{i,j} + f_{i,j+1}), \tag{20}$$

with the matrices $A_{i,j} = \frac{\Delta\tau}{2\Delta\eta^2} \frac{a_j}{s_j^2} - \frac{\Delta\tau}{4\Delta\eta} \frac{b_{i,j} + s'_j \eta_i}{s_j}$, $B_{i,j} = \frac{\Delta\tau}{2} c_{i,j} - \frac{\Delta\tau}{\Delta\eta^2} \frac{a_j}{s_j^2}$ and $C_{i,j} = \frac{\Delta\tau}{2\Delta\eta^2} \frac{a_j}{s_j^2} + \frac{\Delta\tau}{4\Delta\eta} \frac{b_{i,j} + s'_j \eta_i}{s_j}$.

There are three values on the right-hand side of Equation (20): $v_{i-1,j}$, $v_{i,j}$, and $v_{i+1,j}$. Conversely, the values on the left-hand side remain unknown.

For $j = 0$ (i.e. the initial time) and $i = \overline{1, M-1}$, Equation (20) represents a linear system of $M - 1$ equations with $M - 1$ unknown variables, namely $v_{1,1}, v_{2,1}, \dots, v_{M-1,1}$. The first time steps in terms of the initial values $v_{0,0}, v_{1,0}, \dots, v_{n,0}$ and from the Dirichlet boundaries $v_{0,1}$ and $v_{M,1}$ have specific values $\gamma_1(\tau_0)$ and $\gamma_2(\tau_0)$, respectively. We perform a similar procedure for the following iteration time step (τ_j) with $j = \overline{1, N-1}$; that is, for each time step τ_j for $j = \overline{1, N-1}$.

We rewrite Equation (20) in metric form as a $(M - 1) \times (M - 1)$ system of algebraic linear equations (that can be solved by the Gaussian elimination method) as follows:

$$\mathbf{A}v^{n+1} = \mathbf{B}v^n + d, \tag{21}$$

where $v^{n+1} = (v_{1,j+1}, v_{2,j+1}, \dots, v_{M-1,j+1})^t$, $v^n = (v_{1,j}, v_{2,j}, \dots, v_{M-1,j})^t$, and \mathbf{A} and \mathbf{B} are $(M - 1) \times (M - 1)$ matrices as follows:

$$\mathbf{A} = \begin{bmatrix} 1 - B_{1,j+1} & -C_{1,j+1} & 0 \dots \dots 0 & 0 & 0 \\ -A_{2,j+1} & 1 - B_{2,j+1} & -C_{2,j+1} & \dots 0 & 0 \\ \vdots & \vdots & \vdots & & \\ 0 & 0 & 0 \dots -A_{M-2,j+1} & 1 - B_{M-2,j+1} & -C_{M-2,j+1} \\ 0 & 0 & 0 \dots 0 & -A_{M-1,j+1} & 1 - B_{M-1,j+1} \end{bmatrix}$$

$$\mathbf{B} = \begin{bmatrix} 1 + B_{1,j} & C_{1,j} & 0 \dots 0 & 0 & 0 \\ A_{2,j} & 1 + B_{2,j} & C_{2,j} \dots 0 & 0 & 0 \\ \vdots & \vdots & \vdots & & \\ 0 & 0 & 0 \dots A_{M-2,j} & 1 + B_{M-2,j} & C_{M-2,j} \\ 0 & 0 & 0 \dots 0 & A_{M-1,j} & 1 + B_{M-1,j} \end{bmatrix}$$

$$d = \begin{bmatrix} A_{1,j+1}v_{0,j+1} + A_{1,j}v_{0,j} + \frac{\Delta\tau}{2}(f_{1,j} + f_{1,j+1}) \\ \frac{\Delta\tau}{2}(f_{2,j} + f_{2,j+1}) \\ \vdots \\ \frac{\Delta\tau}{2}(f_{M-2,j} + f_{M-2,j+1}) \\ C_{M-1,j+1}v_{M,j+1} + C_{M-1,j}v_{M,j} + \frac{\Delta\tau}{2}(f_{M-1,j} + f_{M-1,j+1}) \end{bmatrix}.$$

The trapezium rule (numerical integration) is applied to discretize Equation (8) ($\ell \in \{0, 1\}$) into different equations:

$$\gamma_3(\tau_j) = \frac{s(\tau_j)}{2N} \left(v_{0,j} + v_{M,j} + 2 \sum_{i=1}^{M-1} v_{i,j} \right), \quad j = \overline{1, N}, \tag{22}$$

$$\gamma_4(\tau_j) = \frac{s^2(\tau_j)}{2N} \left(\eta_0 v_{0,j} + \eta_M v_{M,j} + 2 \sum_{i=1}^{M-1} \eta_i v_{i,j} \right), \quad j = \overline{1, N}. \tag{23}$$

4. Numerical Approximations of the Inverse Problems

In this section, we find the approximated solutions of different quantities of the inverse problem in Equations (1)–(4) in **Case 1** to obtain $\{(u(x, \tau), a(\tau), s(\tau))\}$ when $b(x, \tau)$ is explicitly is given. Then, we find the corresponding solution of the inverse problem in Equations (1)–(4) in **Case 2**, where $\{(u(x, \tau), b(\tau), s(\tau))\}$ require identification when $a(\tau)$ is given.

Handling these inverse problems means solving non-linear optimization problems that minimize the gap between measured data and computed solutions. The minimization of the objective function, subject to the straightforward physical lower-bound constraint $s > 0$, can be achieved by using the *lsqnonlin* non-linear least-square solver from the MATLAB optimization toolbox, which applies the trust region reflective algorithm (TRR) [33,34]. The *lsqnonlin* solver aims to determine the minimum sum of squares by starting from initial guesses. This toolbox routine does not require a supplement of the gradient of the objective function. It uses the TRR algorithm [33,35,36], so it effectively relies on the interior-reflective Newton method. Each iteration results in a large system of linear equations, which we solve by applying the preconditioned conjugate gradient method [37,38].

As we mentioned earlier, **Case 1** concerns finding the thermal diffusivity $a(\tau)$, the free-boundary condition $s(\tau) > 0$ of one-dimensional heat in Equation (1), and the temperature distribution $u(x, \tau)/v(\eta, \tau)$. Equations (14) and (13) are used to calculate $a(0)$ and $s'(0)$, respectively, when the initial time is $\tau = 0$. Given the ill-posed nature of the problem, Tikhonov regularization (ridge regression) can be applied to ensure the suitability and accuracy of the solution [39,40].

From the over-determination conditions in Equation (8) ($\ell \in \{0, 1\}$), we reconstruct Tikhonov’s regularization as follows:

$$J(a, s) := \left\| s(\tau) \int_0^1 v(\eta, \tau) d\eta - \gamma_3(\tau) \right\|^2 + \left\| s^2(\tau) \int_0^1 \eta v(\eta, \tau) d\eta - \gamma_4(\tau) \right\|^2 + \beta_1 \|s(\tau)\|^2 + \beta_2 \|a(\tau)\|^2. \tag{24}$$

The previous Tikhonov regularization functional reconstruction can be expanded and rewritten in the following form:

$$J(\underline{a}, \underline{s}) = \sum_{j=1}^N \left(s_j \int_0^1 v(\eta, \tau_j) d\eta - \gamma_3(\tau_j) \right)^2 + \sum_{j=1}^N \left(s_j^2 \int_0^1 \eta v(\eta, \tau_j) d\eta - \gamma_4(\tau_j) \right)^2 + \beta_1 \sum_{j=1}^N s_j^2 + \beta_2 \sum_{j=1}^N a_j^2. \tag{25}$$

$J(a, \underline{s})$, which is subject to the physical constraints $\underline{s} > 0$ (free boundary) and $\underline{a} > 0$ (thermal diffusivity), is minimized using the optimization package *lsqnonlin*.

We apply the same procedure for **Case 2**, where $a(\tau) = 1$, and we need to identify $b(x, \tau) = b(\tau)$ as well as the free boundary $s(\tau)$ and the temperature $u(x, \tau)/v(\eta, \tau)$. Again, we consider the first initial value for the time $\tau = 0$, which helps to calculate $b(0)$ in Equation (16) and $s'(0)$ in Equation (15). Moreover, we use the over-determination conditions in Equation (8) ($\ell \in \{0, 1\}$) to form the corresponding Tikhonov regularization:

$$G(s, b) := \left\| s(\tau) \int_0^1 v(\eta, \tau) d\eta - \gamma_3(\tau) \right\|^2 + \left\| s^2(\tau) \int_0^1 \eta v(\eta, \tau) d\eta - \gamma_4(\tau) \right\|^2 + \beta_1 \|s(\tau)\|^2 + \beta_2 \|b(\tau)\|^2, \tag{26}$$

which can be rewritten as

$$G(\underline{s}, \underline{b}) = \sum_{j=1}^N \left(s_j \int_0^1 v(\eta, \tau_j) d\eta - \gamma_3(\tau_j) \right)^2 + \sum_{j=1}^N \left(s_j^2 \int_0^1 \eta v(\eta, \tau_j) d\eta - \gamma_4(\tau_j) \right)^2 + \beta_1 \sum_{j=1}^N s_j^2 + \beta_2 \sum_{j=1}^N b_j^2. \tag{27}$$

Then, $G(\underline{s}, \underline{b})$ is minimized using the *lsqnonlin* solver. In both the examined cases, $\beta_i \geq 0$ and $i = 1, 2$ are the regularization parameters identified and regulated according to a specific selection procedure, and the norm is taken in the space $L^2[0, T]$.

To ensure the stability of the inverse solutions, we include random errors (noise) in the input data for Equation (8) ($\ell \in \{0, 1\}$) and monitor the effect of the change.

$$\gamma_3^{\epsilon_1}(\tau_j) = \gamma_3(\tau_j) + \epsilon_{1,j}; \quad \gamma_4^{\epsilon_2}(\tau_j) = \gamma_4(\tau_j) + \epsilon_{2,j}, \quad j = \overline{0, N}, \tag{28}$$

where ϵ_1 and ϵ_2 are arbitrary vectors engendered from a Gaussian normal distribution that has mean zero and standard deviations denoted as σ_1 and σ_2 , respectively:

$$\sigma_1 = p \times \max_{\tau \in [0, T]} |\gamma_3(\tau)|, \quad \sigma_2 = p \times \max_{\tau \in [0, T]} |\gamma_4(\tau)|. \tag{29}$$

The quantity p refers to the percentage of added noise. The MATLAB bulletin function *normrnd* was used to generate the random variables $\underline{\epsilon}_1 = (\epsilon_{1,j})$ and $\underline{\epsilon}_2 = (\epsilon_{2,j})$ for $j = \overline{0, N}$ as follows:

$$\underline{\epsilon}_1 = \text{normrnd}(0, \sigma_1, N), \quad \underline{\epsilon}_2 = \text{normrnd}(0, \sigma_2, N).$$

5. Discussions and Numerical Examples for Cases 1 and 2

In this section, we calculate, discuss, and interpret the numerical results of the time-dependent coefficients $a(\tau)$ and $b(\tau)$ along with $s(\tau) > 0$ and the temperature distribution $v(\eta, \tau)$. We compare the obtained direct solutions with the analytical ones. Because finding the exact solutions to such a problem is not always possible, we run simulations after applying a trim level of noise to the measurements of the direct solver. Then, we seek the best value for the regulation parameters to ensure the accuracy, convergence, and stability of the obtained inverse solutions (reconstructions). We also consider the root mean square error (RMSE), which is given as follows:

$$RMSE(a) = \left[\frac{T}{N} \sum_{j=1}^N (a^{numerical}(\tau_j) - a^{exact}(\tau_j))^2 \right]^{\frac{1}{2}}, \tag{30}$$

$$RMSE(b) = \left[\frac{T}{N} \sum_{j=1}^N (b^{numerical}(\tau_j) - b^{exact}(\tau_j))^2 \right]^{\frac{1}{2}}, \tag{31}$$

$$RMSE(s) = \left[\frac{T}{N} \sum_{j=1}^N (s^{numerical}(\tau_j) - s^{exact}(\tau_j))^2 \right]^{\frac{1}{2}}. \tag{32}$$

We use the RMSE regression method to understand the relationships between $a^{numerical}$, $b^{numerical}$, and $s^{numerical}$ (the predicted values) and a^{exact} , b^{exact} , and s^{exact} (the observed values), respectively, for the j^{th} observation. For simplicity, we fix $T = 1$ throughout the simulations.

5.1. Numerical Example for Case 1

Considering the data inputs in the work of Hussein and Lesnic [41], we define

$$a(\tau) = \sqrt{1 + \tau}, \quad c(x, \tau) = 0, \quad b(x, \tau) = 0, \quad s(\tau) = \sqrt{2 - \tau}, \quad f(x, \tau) = 8 - 2\sqrt{1 + \tau}, \tag{33}$$

$$u(x, \tau) = 8\tau + (1 + x)^2.$$

Inserting the exact value of $u(x, \tau)$ into the integral in Equation (4) ($\ell \in \{0, 1\}$) helps to analytically compute $\gamma_3(\tau)$ and $\gamma_4(\tau)$. Thus,

$$\gamma_3(\tau) = \int_0^{s(\tau)} u(x, \tau) dx = \sqrt{2 - \tau} \left(\frac{5}{3} + \sqrt{2 - \tau} + \frac{23\tau}{3} \right), \tag{34}$$

$$\gamma_4(\tau) = \int_0^{s(\tau)} xu(x, \tau) dx = (2 - \tau) \left(1 + \frac{2\sqrt{2 - \tau}}{3} + \frac{15\tau}{4} \right), \tag{35}$$

and using the earlier transformation

$$\eta = \frac{x}{s(\tau)} = \frac{x}{\sqrt{2 - \tau}}$$

allows us to analytically calculate the exact values of $v(y, \tau)$ and $f(y, \tau)$. This leads to

$$v(\eta, \tau) = 8\tau + (1 + \eta\sqrt{2 - \tau})^2, \quad f(\eta, \tau) = 8 - 2\sqrt{1 + \tau}, \tag{36}$$

which involves the inchoate and boundary conditions in Equations (6) and (7) and results in the following defined functions:

$$\varphi(\eta) = (1 + \sqrt{2}\eta)^2; \quad \gamma_1(\tau) = u(0, \tau) = 1 + 8\tau; \quad \gamma_2(\tau) = u(s(\tau), \tau) = (1 + \sqrt{2 - \tau})^2.$$

For the transformed direct problem in Equations (5)–(8), $\gamma_3(\tau)$ and $\gamma_4(\tau)$ can be calculated numerically using the trapezium rule as shown in Equations (22) and (23). Tables 1 and 2 compare the exact values of $\gamma_3(\tau)$ and $\gamma_4(\tau)$, which are defined in Equations (34) and (35) respectively, and the corresponding numerical values approximated via CN techniques (Equations (22) and (23)) at equally-spaced time steps in the interval $\tau \in (0, 1)$.

We focus on solving the inverse problem in Equations (5)–(8) in **Case 1**. When $b(x, \tau)$ is given, the functions $s(\tau)$ and $a(\tau)$ must be detected using the previous data inputs. We set initial guesses for $s(\tau)$ and $a(\tau)$ at $\tau = 0$ to start the optimization procedure. We achieve this by using Equations (13) and (14), respectively. Therefore, $\underline{s}(0) = \underline{s}_0 = \sqrt{2}$ and $\underline{a}(0) = 1$. We work with this particular example because all of the conditions in Theorem 1 are met, which ensures the existence and uniqueness of the inverse solutions.

Table 1. Real and numerically approximated values of $\gamma_3(\tau)$ at various times and mesh sizes.

τ	0.1	0.2	0.3	0.4	0.5	0.6	0.7	0.8	0.9
$M = N = 10$ (Relative error)	2.2585 (57.01452%)	6.0973 (0.06565%)	6.8756 (0.05384%)	7.5906 (0.04481%)	8.2391 (0.03643%)	8.8176 (0.03176%)	9.3217 (0.02683%)	9.7466 (0.02155%)	10.0867 (0.01884%)
$M = N = 20$ (Relative error)	5.2552 (0.02093%)	6.0943 (0.01641%)	6.8728 (0.01309%)	7.5881 (0.01186%)	8.2369 (0.00971%)	8.8155 (0.00794%)	9.3198 (0.00644%)	9.745 (0.00513%)	10.0853 (0.00496%)
$M = N = 40$ (Relative error)	5.2544 (0.00571%)	6.0935 (0.00328%)	6.8721 (0.00291%)	7.5875 (0.00395%)	8.2363 (0.00243%)	8.815 (0.00227%)	9.3194 (0.00215%)	9.7446 (0.00103%)	10.0849 (0.00099%)
$M = N = 80$ (Relative error)	5.2542 (0.00190%)	6.0933 (0%)	6.872 (0.00146%)	7.5873 (0.00132%)	8.2361 (0%)	8.8149 (0.00113%)	9.3193 (0.00107%)	9.7445 (0%)	10.0848 (0%)
Exact	5.2541	6.0933	6.8719	7.5872	8.2361	8.8148	9.3192	9.7445	10.0848

Table 2. Real and numerically approximated values of $\gamma_4(\tau)$ at various times and mesh sizes.

τ	0.1	0.2	0.3	0.4	0.5	0.6	0.7	0.8	0.9
$M = N = 10$ (Relative error)	4.3762 (0.40610%)	4.7761 (0.33824%)	5.1048 (0.28683%)	5.3624 (0.24677%)	5.549 (0.21310%)	5.6647 (0.18393%)	5.7098 (0.15963%)	5.6843 (0.13917%)	5.5885 (0.12362%)
$M = N = 20$ (Relative error)	4.3629 (0.10095%)	4.764 (0.08403%)	5.0938 (0.07072%)	5.3525 (0.06169%)	5.5402 (0.05418%)	5.6569 (0.04598%)	5.7029 (0.03859%)	5.6783 (0.03347%)	5.5833 (0.0305%)
$M = N = 40$ (Relative error)	4.3592 (0.01606%)	4.761 (0.02101%)	5.0911 (0.01769%)	5.3501 (0.01682%)	5.538 (0.01445%)	5.655 (0.01238%)	5.7012 (0.00877%)	5.6769 (0.00881%)	5.5821 (0.00896%)
$M = N = 80$ (Relative error)	4.3588 (0.00689%)	4.7602 (0.00420%)	5.0904 (0.00393%)	5.3494 (0.00374%)	5.5374 (0.00361%)	5.6545 (0.00354%)	5.7008 (0.00175%)	5.6765 (0.00176%)	5.5817 (0.00179%)
Exact	4.3585	4.76	5.0902	5.3492	5.5372	5.6543	5.7007	5.6764	5.5816

We use the same data inputs above (Equation (33)) and consider the numerical estimations of γ_3 and γ_4 when there is no noise applied to Equation (28). Then, we visualize the minimized objective function in Equation (25) against the number of iterations when the regularization parameters β_1 and β_2 are set to zero. Figure 1 shows a fast convergence on the measured minimized objective function as the number of iterations rises, reaching a monotonic stage in 31 iterations. The non-regularized objective function’s curve diminishes rapidly in the first five iterations and then reaches a steady stage with a high order of accuracy of $O(10^{-9})$.

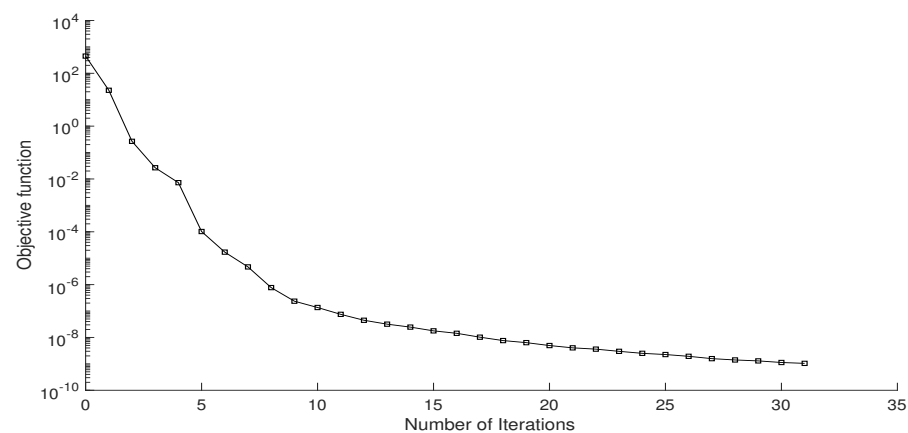


Figure 1. Visualization of the minimized objective function defined in Equation (25) when no noise is imposed and no regularization is applied.

The associated numerical solutions for the unknown functions $s(\tau)$ and $a(\tau)$ are calculated simultaneously and plotted in Figure 2a and b, respectively.

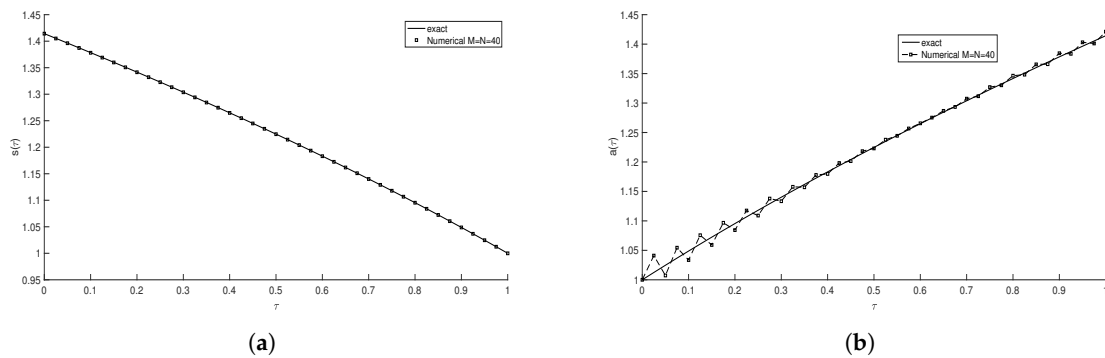


Figure 2. Exact solutions (solid lines) and numerical solutions (squares) for (a) $s(\tau)$ and (b) $a(\tau)$ when noise and regularization are not applied.

We successfully retrieve an accurate and steady solution for the free-boundary function $s(\tau)$. Figure 2 shows minor instability in the thermal diffusivity values of the function $a(\tau)$ close to both edges. The oscillations are more evident on the left-hand side of the approximated $a(\tau)$, increasing as the time gets closer to zero. Consequently, $s(\tau)$ does not need to be regularized. Hence, we fix $\beta_1 = 0$ in Equation (25) and use the Tikhonov regularization method for $a(\tau)$.

Next, we find the inverse solution for **Case 1** when a small level of noise of $\epsilon = 0.01\%$ is included in the over-determination conditions $\gamma_3(\tau)$ and $\gamma_4(\tau)$, as in Equation (28). We emphasize that the regularization procedure has not yet been used to solve the problem. Figure 3 shows the objective minimization function against the number of iterations when noise is applied. The figure illustrates that the non-regularized objective function’s convergence is fast in the first few iterations, settled in the next few, and then becomes steady. The objective function reaches a stationary stage in 140 iterations, with a high order of accuracy of $O(10^{-7})$. Not considering the exact solutions of $\gamma_3(\tau)$ and $\gamma_4(\tau)$ and applying some noise to them results in a slower convergence and a lower level of accuracy, as seen by comparing the minimized objective functions shown in Figures 1 and 3.

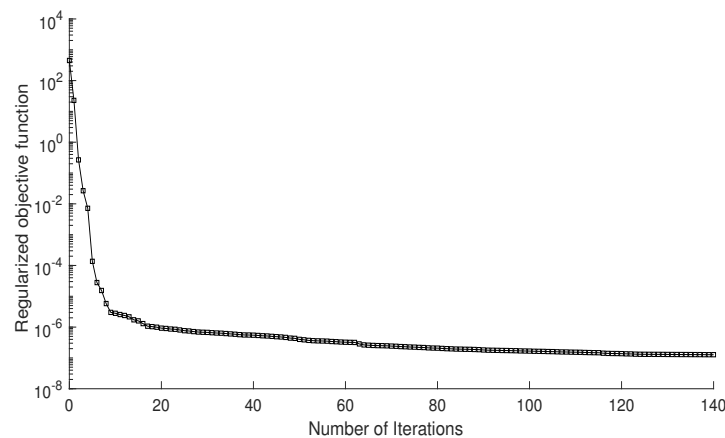


Figure 3. Visualization of the minimized objective function defined in Equation (25) when the noise level $\epsilon = 0.01\%$ is imposed and no regularization is applied.

Exploring the associated numerical results in Figure 4 illustrates that the free boundary maintains stability, while the thermal diffusivity shows more severe oscillatory behavior compared to Figure 2b.

Finally, we apply the Tikhonov regularization method to obtain a stable, accurate, and efficient reconstruction for the unknown function $a(\tau)$. The L-curve method, the RMSE

curve, and trial and error are used to identify the most appropriate regularization parameter β_2 [15,42–44].

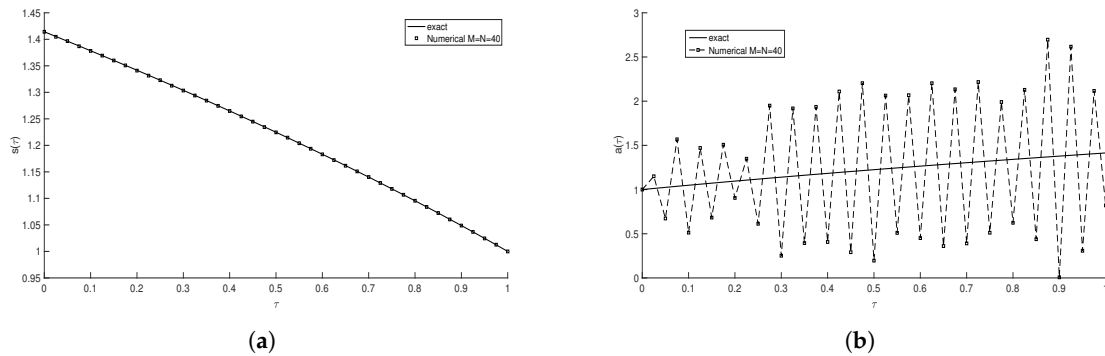


Figure 4. Real and numerically approximated values for (a) $s(\tau)$ and (b) $a(\tau)$ with noise level $\epsilon = 0.01\%$ and no regularization applied.

Finding the optimal value of the regularization parameter using the L-curve method is impossible since we cannot see the L-shaped curve in the line graph in Figure 5. Instead, we apply the RMSE regression method; as shown in Figure 6, the curve’s minimum value occurs at $\beta_2 = 10^{-4}$. Thus, β_2 is considered an optimal value of the regularization parameter to obtain the best numerical values for $a(\tau)$.

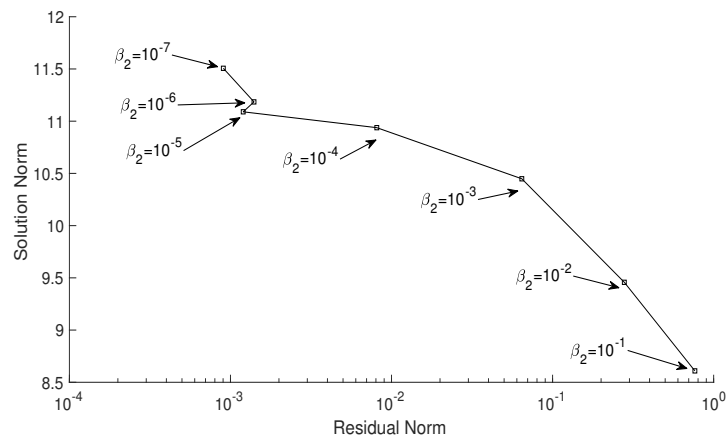


Figure 5. L–curve line graph where potential values for β_2 are tested and the noise level $\epsilon = 0.01\%$ is imposed.

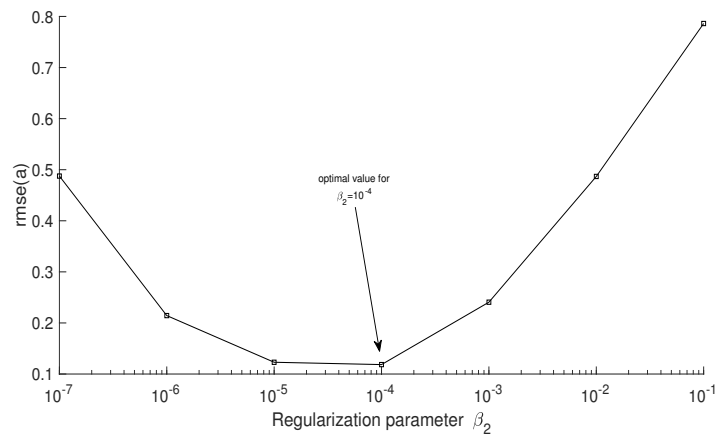


Figure 6. Minimum RMSE line graph where potential values for β_2 are tested and the noise level $\epsilon = 0.01\%$ is imposed.

Figure 7 shows the calculated minimized objective functions using Equation (25) against the number of iterations when the regularization parameter β_2 is set to 10^{-3} , 10^{-4} , and 10^{-5} . The objective function with $\beta_2 = 10^{-4}$ converges faster than the others and reaches a steady distribution in 10 iterations, taking 380 seconds. The objective functions with $\beta_2 = 10^{-3}$ and $\beta_2 = 10^{-5}$ have slower convergences and reach their stationary distributions in 12 iterations after 447 and 449 seconds, respectively.

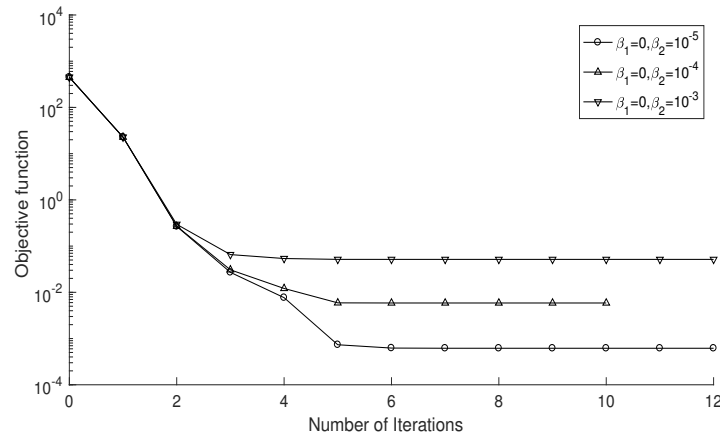
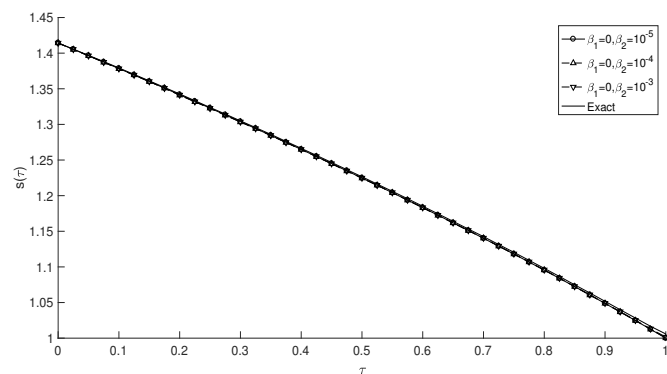
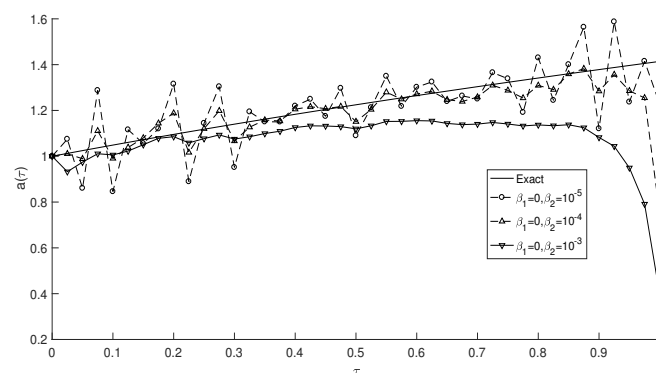


Figure 7. Visualization of the minimized objective function defined in Equation (25) when the noise level $\epsilon = 0.01\%$ is imposed and various regularization parameters are considered.

Figure 8 illustrates the reconstructions of the inverse solutions $s(\tau)$ and $a(\tau)$ in Case 1, taking into account various regularization parameters, including the optimal value.



(a)



(b)

Figure 8. Real and numerically approximated values for (a) $s(\tau)$ and (b) $a(\tau)$ with $p = 0.01\%$ noise and various regularization parameters for Case 1.

The free-boundary function $s(\tau)$ is estimated very well even when its corresponding regularization parameter is set to zero, $\beta_1 = 0$. Since the reconstruction is performed simultaneously for all model parameters, selecting the best regularization parameter for the thermal diffusivity $a(\tau)$ positively impacts the obtained free-boundary values; this is evident in the right-hand side of the curve in Figure 8a. Moreover, $\beta_2 = 10^{-4}$ has significantly smoothed $a(\tau)$ and increased the solutions' accuracy compared to the other examined regularization parameters.

5.2. Numerical Example For Case 2

In this section, we solve the inverse problem stated in Equations (5)–(8) for **Case 2**, where $s(\tau)$ and $b(\tau)$ are unknown functions and the temperature is $v(\eta, \tau)$. We solve this inverse problem with fed-in data:

$$\begin{aligned} \varphi(\eta) &= (1 + \eta)^2, \quad \gamma_1(\tau) = 1 + 10\tau, \quad \gamma_2(\tau) = 10t + (2 + \tau)^2 \\ f(\eta, \tau) &= 8 - 2(-1 - \tau)(1 + (1 + \tau)\eta), \\ \gamma_3(\tau) &= (1 + \tau) \left(\frac{7}{3} + \frac{35\tau}{3} + \frac{\tau^2}{3} \right), \quad \tau \in [0, T] \\ \gamma_4(\tau) &= \int_0^{s(\tau)} xu(x, \tau)dx = \frac{1}{12}(1 + \tau)^2(17 + 74\tau + 3\tau^2), \quad \tau \in [0, T]. \end{aligned}$$

The exact and numerical values for input data γ_3 and γ_4 with their relative errors are listed in Tables 3 and 4, respectively. The conditions in Theorems 2 and 3 concerning the uniqueness and existence of the solution hold. Therefore, the local existence and uniqueness of the solution are guaranteed. The analytical solution of this problem is provided as follows:

$$u(x, \tau) = 10\tau + (1 + x)^2, \quad b(\tau) = -1 - \tau, \quad s(t) = 1 + \tau,$$

and the transformed solution is

$$v(\eta, \tau) = 10\tau + (1 + (1 + \tau)\eta)^2, \quad b(\tau) = -1 - \tau, \quad s(\tau) = 1 + \tau. \tag{37}$$

At the beginning of our investigation, we started with a noise-free case, i.e., $p = 0$ in Equation (28). Figure 9 shows the objective function in Equation (27) as a function of the number of iterations where no regularization is applied, i.e., $\beta_1 = \beta_2 = 0$. The figure shows the speedy convergence of the minimization problem toward local minima with a meagre value of order $O(10^{-9})$ in 19 iterations. The corresponding numerical results are presented in Figure 10. From this figure, we can see the overlap between the exact and numerical solutions of the unknown functions $s(\tau)$ and $b(\tau)$, which indicates an excellent agreement with $RMSE(b) = 7.9 \times 10^{-4}$ and $RMSE(h) = 4.9 \times 10^{-5}$ from Equations (31) and (32), respectively.

Table 3. Real and numerically approximated solutions of $\gamma_3(\tau)$ at various times and mesh sizes for the direct problem.

τ	0.1	0.2	0.3	0.4	0.5	0.6	0.7	0.8	0.9
$N = M = 10$ (Relative error)	3.8559 (0.05709%)	5.6189 (0.05164%)	7.626 (0.04854%)	9.8792 (0.04557%)	12.3806 (0.04525%)	15.1322 (0.04562%)	18.1359 (0.04523%)	21.3937 (0.045361%)	24.9078 (0.04619%)
$N = M = 20$ (Relative error)	3.8542 (0.01297%)	5.6167 (0.01246%)	7.6232 (0.01181%)	9.8758 (0.01114%)	12.3764 (0.01131%)	15.127 (0.01124%)	18.1297 (0.01103%)	21.3864 (0.01122%)	24.8992 (0.01165%)
$N = M = 40$ (Relative error)	3.8538 (0.00259%)	5.6162 (0.00356%)	7.6226 (0.00394%)	9.875 (0.00304%)	12.3754 (0.00323%)	15.1258 (0.00331%)	18.1282 (0.00276%)	21.3846 (0.00281%)	24.897 (0.00282%)
$N = M = 80$ (Relative error)	3.8537 (0%)	5.616 (0%)	7.6224 (0.00131%)	9.8747 (0%)	12.3751 (0.00081%)	15.1254 (0.00066%)	18.1278 (0.00055%)	21.3842 (0.00094%)	24.8965 (0.00080%)
Exact	3.8537	5.616	7.6223	9.8747	12.375	15.1253	18.1277	21.384	24.8963

Table 4. Real and numerically approximated solutions of $\gamma_4(\tau)$ at various times and mesh sizes for the direct problem.

τ	0.1	0.2	0.3	0.4	0.5	0.6	0.7	0.8	0.9
$N = M = 10$	2.4715	3.8413	5.5732	7.7085	10.2895	13.3591	16.9606	21.1381	25.9361
(Relative error)	(0.32881%)	(0.28457%)	(0.26085%)	(0.24448%)	(0.23282%)	(0.22507%)	(0.21981%)	(0.21667%)	0.21406%
$N = M = 20$	2.4654	3.8331	5.5623	7.6944	10.2716	13.3366	16.9327	21.1038	25.8946
(Relative error)	(0.08119%)	(0.07049%)	(0.06476%)	(0.06112%)	(0.05844%)	(0.05627%)	(0.05495%)	(0.05405%)	(0.05371%)
$N = M = 40$	2.4639	3.8311	5.5596	7.6909	10.2671	13.3309	16.9257	21.0953	25.8842
(Relative error)	(0.02029%)	(0.01827%)	(0.01619%)	(0.01561%)	(0.01461%)	(0.01350%)	(0.01359%)	(0.01375%)	(0.01352%)
$N = M = 80$	2.4635	3.8306	5.5589	7.69	10.266	13.3295	16.9239	21.0931	25.8816
(Relative error)	(0.0041%)	(0.00522%)	(0.00359%)	(0.00390%)	(0.00389%)	(0.00300%)	(0.00295%)	(0.00332%)	(0.00348%)
Exact	2.4634	3.8304	5.5587	7.6897	10.2656	13.3291	16.9234	21.0924	25.8807

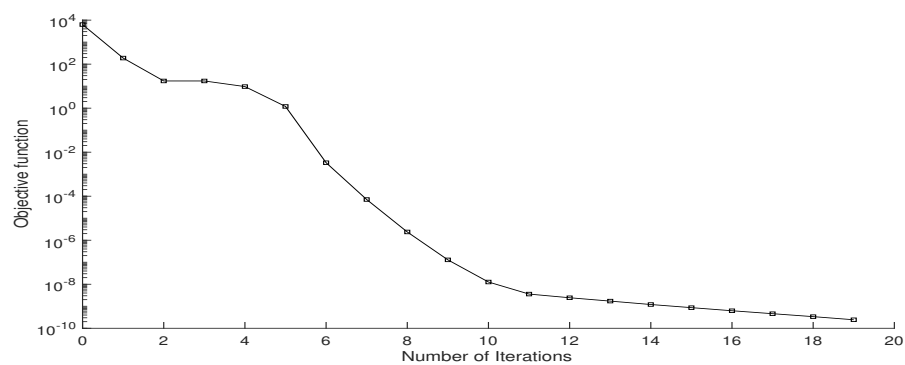


Figure 9. The objective function in Equation (27) when noise and regularization are not applied in Case 2.

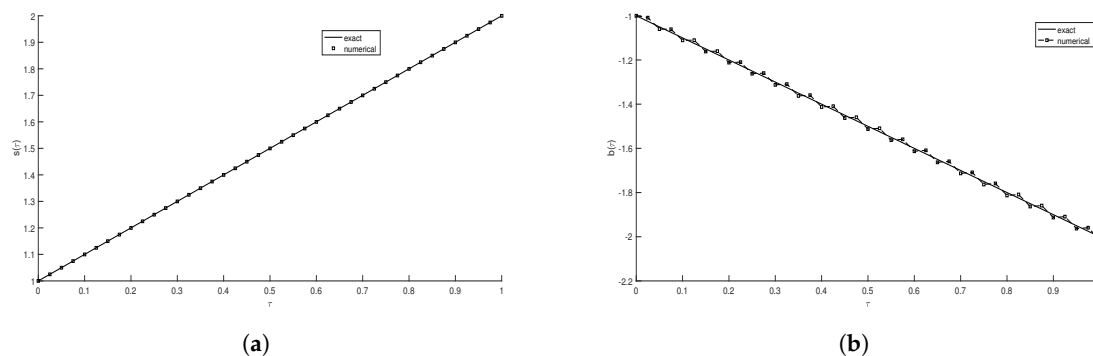


Figure 10. Actual and numerically approximated solutions for (a) $s(\tau)$ and (b) $b(\tau)$ when noise and regularization are not applied in Case 2.

Figure 10b displays the numerical solution of $s(\tau)$, which nearly follows their corresponding precise solutions, with some noticeable small instability despite not yet applying any errors/noise in the inputs. When we add $p = 0.01\%$ noise to the input data in Equation (28), the solutions often follow the same pattern as in Case 1. As shown in Figure 11, we obtain an accurate and stable solution for $s(\tau)$ and an unstable solution for $b(\tau)$, indicating that regularization is necessary.

We expect such unusable behavior of the calculated solution because we are investigating an ill-posed problem. A small error in the input data (γ_3, γ_4) leads to major errors in the output solutions ($s(\tau), b(\tau)$). Regularization should be applied to overcome this difficulty. We apply Tikhonov regularization by adding a penalty term ($\beta_1 \|s\|^2 + \beta_2 \|b\|^2$) to the objective function in Equation (27).

Similar to the corresponding case in Case 1, noise does not affect $s(\tau)$. By contrast, $b(\tau)$ applies regularization on $b(\tau)$ only and fixes $\beta_1 = 0$. To obtain the optimal regularization parameter β_2 , which gives accurate and stable results, different selection methods were considered. These include the L-curve method, minimum RMSE, and trial and error using Equations (31) and (32). Figures 12 and 13 present the L-curve plot and the minimum RMSE values as a function of the regularization parameter β_2 , respectively. From these figures, it can be concluded that the best choice for β_2 is 10^{-3} , which has the lowest value of $RMSE(b)$. The objective function in Equation (27) is plotted for some $\beta_2 \in \{10^{-5}, 10^{-4}, 10^{-3}, 10^{-2}\}$ in Figure 14.

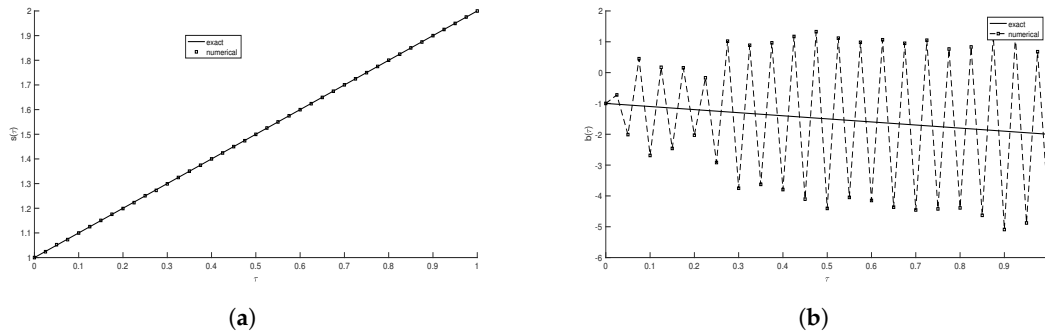


Figure 11. Actual and numerically approximated solutions for (a) $s(\tau)$ and (b) $b(\tau)$ where $p = 0.01\%$ noise is included and no regularization is applied in Case 2.

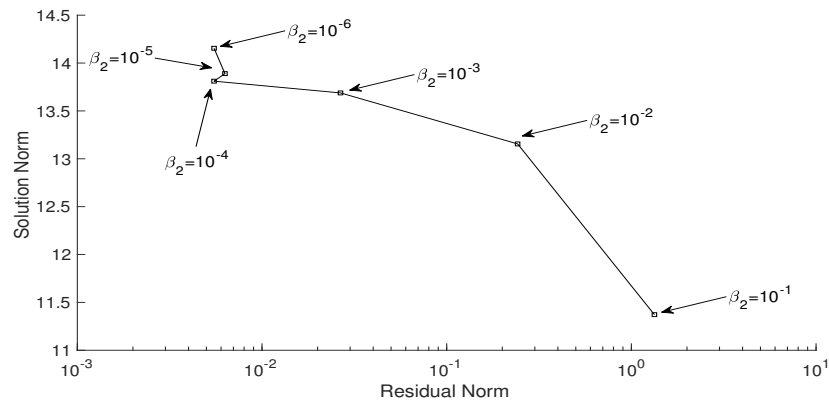


Figure 12. L-curve plot for the second inverse problem with $p = 0.01\%$ noise and regularization for Case 2.

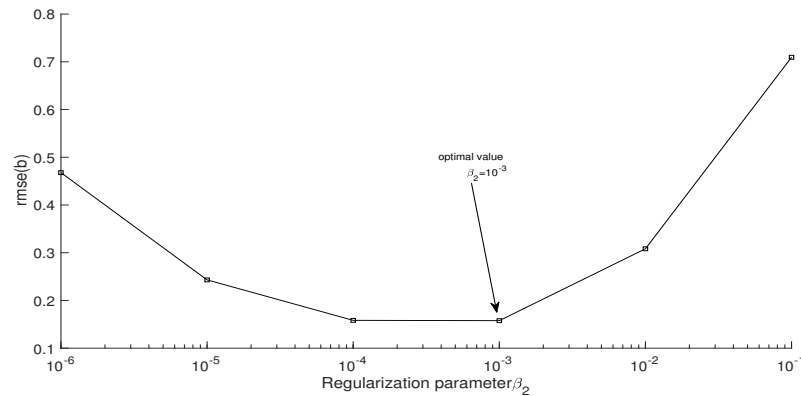


Figure 13. Minimum RMSE plot for the second inverse problem with $p = 0.01\%$ noise (potential measurement errors) and regularization for Case 2.

From Figures 12 and 13, one can conclude that the optimal choice for β_2 is 10^{-3} ; this is also clear in Figure 15.

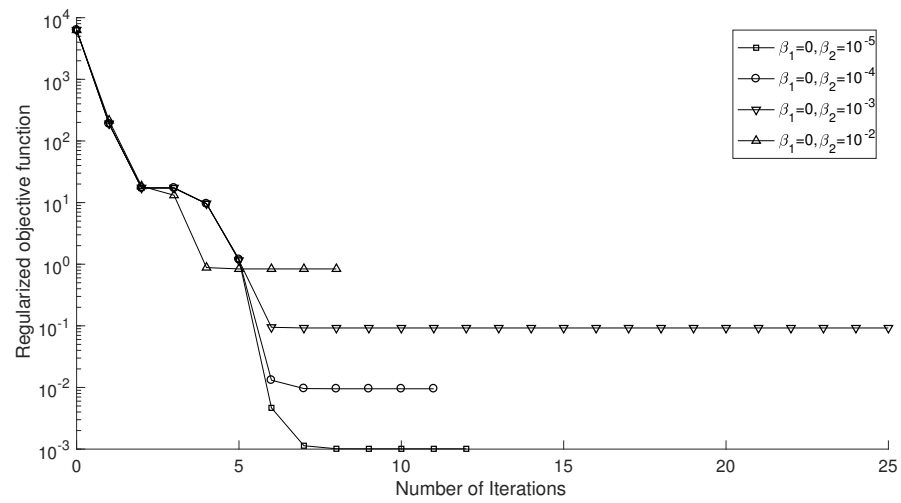
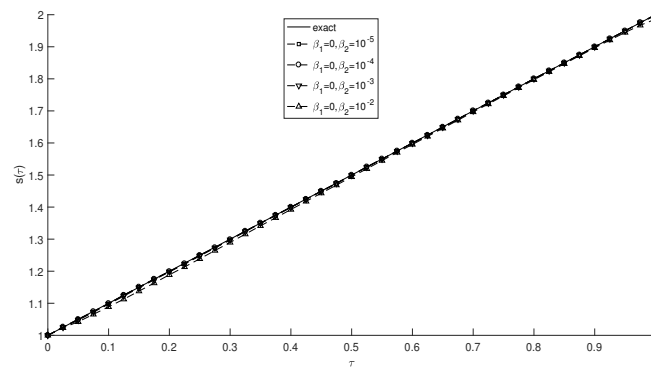
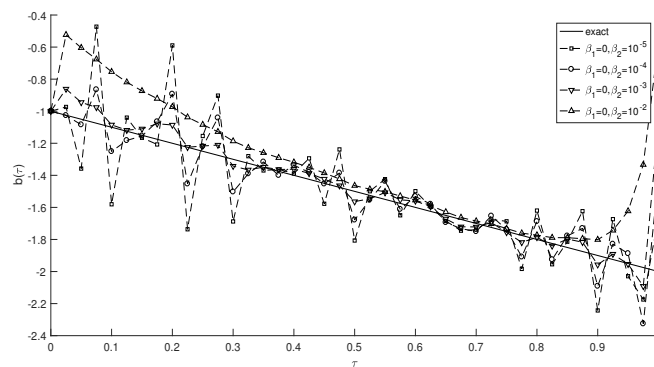


Figure 14. The regularized objective function in Equation (27) for the second inverse problem with $p = 0.01\%$ noise (potential measurement errors) and regularization for Case 2.



(a)



(b)

Figure 15. Actual and numerically approximated solutions for (a) $s(\tau)$ and (b) $b(\tau)$ with $p = 0.01\%$ noise (potential measurement errors) and regularization for Case 2.

6. Conclusions

This research describes a successful approach to finding the numerical solutions (temperature distributions, free boundary, and thermal diffusivity or advection velocities) to time-dependent free-boundary inverse coefficient problems while ensuring the approximations' existence, uniqueness, and reliability. First, we converted the moving boundary function to a fixed domain function by choosing a simple transformation. Then, due to the unconditional stability and convergence of the Crank–Nicholson finite difference scheme, we used it to solve the forward problem (an initial boundary value problem). The obtained numerical values of non-localized integral observations, $\gamma_3(\tau)$ and $\gamma_4(\tau)$ in the over-determined conditions, are used to generate and feed in the reconstruction code, which uses the *lsqnonlin* non-linear least-square optimization routine. This MATLAB toolbox uses the trust region reflective algorithm based on the inner-reflective Newton technique and does not call for an additional gradient for the objective function. We used the Tikhonov regularization approach (ridge regression) to overcome the problem's ill-posed nature, ensuring the solution's applicability and correctness. We also used the root mean square error and L-curve to test and select the optimal values for the regularization parameters to obtain excellent approximations, as the numerical examples show. The numerical approach in this paper could be extended to two- or three-dimensional problems. Additionally, future studies could consider time- and spatial-dependent coefficient identification problems. Moreover, deep learning techniques could be integrated into the mathematical methods used in this work to increase the speed and accuracy of solutions for such inverse problems.

Author Contributions: Conceptualization, M.S.H. and S.O.H.; methodology, T.E.D.; software, M.S.H.; validation, T.E.D. and S.O.H.; formal analysis, M.S.H. and M.Q.; investigation, M.S.H.; resources, T.E.D.; data curation, M.S.H.; writing—original draft, M.S.H., T.E.D., S.O.H. and M.Q.; writing—review and editing, T.E.D. and S.O.H.; visualization, M.Q.; supervision, M.S.H. and T.E.D.; project administration, T.E.D.; funding acquisition, T.E.D. All authors have read and agreed to the published version of the manuscript.

Funding: This research was funded by Department of Computing and Mathematics, Faculty of Science and Engineering, Manchester Metropolitan University, Manchester, UK (grant number).

Data Availability Statement: The original contributions presented in the study are included in the article, further inquiries can be directed to the corresponding authors.

Conflicts of Interest: The authors declare no conflict of interest.

Abbreviations

The following abbreviations are used in this manuscript:

CN	Crank–Nicolson finite difference method
L^2	Euclidean norm
FDM	Finite difference method
ICP	Initial condition problem
lsqnonlin	Optimization tool
PDE	Partial differential equation
RMSE	Root mean square error
C^2	The C refers to a continuous function, and 2 the times its derivative is continuous
TRR	Trust region reflective

References

1. Glotov, D.; Hames, W.E.; Meirc, A.J.; Ngoma, S. An integral constrained parabolic problem with applications in their thermochronology. *Comp. Math. Appl.* **2016**, *71*, 2301–2312.
2. Čiupaila, R.; Sapagovas, M.; Štikonienė, O. Numerical solution of nonlinear elliptic equation with nonlocal condition. *Non-Linear Anal. Model. Control* **2013**, *18*, 412–426.
3. Hazanee, A.; Lesnic, D. Determination of a time-dependent coefficient in the bioheat equation. *Int. J. Mech. Sci.* **2014**, *88*, 259–266.

4. Hussein, S.O.; Dyhoum, T.E. Solutions for non-homogeneous wave equations subject to unusual and Neumann boundary conditions. *J. Appl. Math.* **2022**, *430*, 127–285.
5. Cao, K.; Lesnic, D. Simultaneous reconstruction of the spatially-distributed reaction coefficient, initial temperature and heat source from temperature measurements at different times. *Comput. Math. Appl.* **2019**, *78*, 3237–3249.
6. Liu, W.; Wang, B. A local meshless method for two classes of parabolic inverse problems. *J. Appl. Math. Phys.* **2018**, *6*, 968–978.
7. Huang, D.; Li, Y.; Pei, D. Identification of a time-dependent coefficient in heat conduction problem by new iteration method. *Adv. Math. Phys.* **2018**, *2018*, 1–7.
8. Mishra, A. Thompson and Troian slip effects on ternary hybrid nanofluid flow over a permeable plate with chemical reaction. *Numer. Heat Transf. Part B Fundam.* **2024**, 1–29. <https://doi.org/10.1080/10407790.2024.2346929>.
9. Hussein, S.O.; Lesnic, D.; Yamamoto, M. Reconstruction of space-dependent potential and/or damping coefficients in the wave equation. *Comput. Math. Appl.* **2017**, *74*, 1435–1454.
10. Dyhoum, T.E.; Aykroyd, R.G.; Lesnic, D. Detection of multiple rigid inclusions from ERT data using the complete-electrode model. *IJTS* **2017**, *30*, 64–86.
11. Dehghan, M. Implicit collocation technique for the heat equation with the non-classic initial condition. *Int. J. Nonlinear Sci. Numer.* **2006**, *7*, 461–466.
12. Mazraeh, H.D.; Pourgholi, R.; Tavana, S. The fully-implicit finite difference method for solving nonlinear inverse parabolic problems with unknown source term. *Int. J. Comput. Sci.* **2018**, *9*, 405–418.
13. Iijima, K. Numerical solution of backward heat conduction problems by a high order lattice-free finite difference method. *J. Chin. Inst. Eng.* **2004**, *27*, 611–620.
14. Fu, C.-L.; Xiang-Tuan, X.; Qian, Z. Fourier regularization for a backward heat equation. *J. Math. Anal. Appl.* **2007**, *331*, 472–480.
15. Damirchi, J.; Yazdani, A.R.; Shamami, T.R.; Hasanpour, M. Numerical investigation of an inverse problem based on regularization method. *Math. Sci.* **2019**, *13*, 193–199.
16. Lesnic, D.; Elliott, L.; Ingham, D.B. An iterative boundary element method for solving the backward heat conduction problem using an elliptic approximation. *Inverse Probl. Sci. Eng.* **1998**, *6*, 255–279.
17. Mera, N.S.; Elliott, L.; Ingham, D.B.; Lesnic, D. An iterative boundary element method for solving the one-dimensional backward heat conduction problem. *Int. J. Heat Mass Transf.* **2001**, *44*, 1937–1946.
18. Friedman, A. Free boundary problems in science and technology. *Not. Am. Math. Soc.* **2000**, *47*, 854–861.
19. Słota, D. Direct and inverse one-phase Stefan problem solved by the variational iteration method. *Comput. Math. Appl.* **2007**, *54*, 1139–1146.
20. Wang, S.; Perdikaris, P. Deep learning of free boundary and Stefan problems. *J. Comput. Phys.* **2020**, *428*, 109914.
21. Hryntsiw, N. The inverse problem with free boundary for a weakly degenerate parabolic equation. *J. Math. Sci.* **2012**, *183*, 779–795.
22. Huzyk, N. Inverse problem of determining the coefficients in a degenerate parabolic equation, *Electron. J. Differ. Equ.* **2014**, *2014*, 1–11.
23. Huzyk, N. Determination of the lower coefficient in a parabolic equation with substantial degeneration. *Ukr. Math. J.* **2016**, *68*, 1049–1061.
24. Martín-Vaquero, J.; Sajavičius, S. The two-level finite difference schemes for the heat equation with nonlocal initial condition. *Appl. Math. Comput.* **2019**, *342*, 166–177.
25. Daftardar-Gejji, V.; Jafari, H. An iterative method for solving nonlinear functional equations. *J. Math. Anal. Appl.* **2006**, *316*, 753–763.
26. Huntul, M.J.; Lesnic, D. Determination of a time-dependent free boundary in a two-dimensional parabolic problem. *Int. J. Appl. Comput.* **2019**, *3*, 118–132.
27. Huntul, M.J.; Lesnic, D. Determination of the time-dependent convection coefficient in two-dimensional free boundary problems. *Eng. Comput.* **2021**, *38*, 3694–3709.
28. Qassim, M.; Hussein, M.S. Numerical solution to recover time-dependent coefficient and free boundary from nonlocal and Stefan type overdetermination conditions in heat equation. *IJS* **2022**, *63*, 147–155.
29. Adil, Z.; Hussein, M.S.; Lesnic, D. Determination of time-dependent coefficients in moving boundary problems under nonlocal and heat moment observations. *JCMSE* **2021**, *22*, 500–513.
30. Dyhoum, T.E. Finite Difference Methods for Solving One and Two-Dimensional Heat Equation. Master's Thesis, Misurata University, Misurata, Libya, 2008.
31. Lin, Y. Analytical and numerical solutions for a nonlocal nonlinear parabolic differential equations class. *SIAM J. Math. Anal.* **1994**, *25*, 577–1594.
32. Liu, J.; Hao, Y. Crank–Nicolson method for solving uncertain heat equation. *Soft. Comput.* **2022**, *26*, 937–945.
33. Coleman, T.F.; Li, Y. On the convergence of interior-reflective Newton methods for nonlinear minimization subject to bounds. *Math. Program.* **1994**, *67*, 189–224.
34. Coleman, T.F.; Verma, A. A preconditioned conjugate gradient approach to linear equality constrained minimization. *Comput. Optim. Appl.* **2001**, *20*, 61–72.
35. Coleman, T.F.; Li, Y. An interior trust region approach for nonlinear minimization subject to bounds. *SIAM J. Optim.* **1996**, *6*, 418–445.
36. Yuan, Y.X. Recent advances in trust region algorithms. *Math. Program.* **2015**, *151*, 249–281.

37. Mathworks, Documentation Optimization Toolbox. 2019. Available online: www.mathworks.com/help/toolbox/optim/ug/brnoybu.html (accessed on 16 September 2019).
38. Manasi, T.; Sathish, V. Pipelined preconditioned conjugate gradient methods for real and complex linear systems for distributed memory architectures. *J. Parallel Distrib. Comput.* **2022**, *163*, 147–155.
39. Kress, R. Tikhonov Regularization. In *Linear Integral Equations*; Applied Mathematical Sciences; Springer: New York, NY, USA, 2014; Volume 82. https://doi.org/10.1007/978-1-4614-9593-2_16.
40. Shraddha, M.N.; Prasad, K.J.R.; Venkatanareshbabu, K. Fractional Tikhonov regularization to improve the performance of extreme learning machines. *Phys. A Stat. Mech. Appl.* **2020**, *551*, 0378–4371.
41. Hussein, M.S.; Lesnic, D. Determination of a time-dependent thermal diffusivity and free boundary in heat conduction. *Int. Commun. Heat Mass Transf.* **2014**, *53*, 154–163.
42. Belge, M.; Kilmer, M.E.; Miller, E.L. Efficient determination of multiple regularization parameters in a generalized L-curve framework. *Inverse Probl.* **2002**, *18*, 1161–1183.
43. Engl, H.; Grever, W. Using the L-curve for determining optimal regularization parameters. *Numer. Math.* **1994**, *69*, 25–31.
44. Liu, S.; Zhang, J. Machine-learning-based prediction of regularization parameters for seismic inverse problems. *Acta. Geophys.* **2021**, *69*, 809–820.

Disclaimer/Publisher’s Note: The statements, opinions and data contained in all publications are solely those of the individual author(s) and contributor(s) and not of MDPI and/or the editor(s). MDPI and/or the editor(s) disclaim responsibility for any injury to people or property resulting from any ideas, methods, instructions or products referred to in the content.